Fabricating High Performance, Donor–Acceptor Copolymer Solar Cells by Spray-Coating in Air

Tao Wang, Nicholas W. Scarratt, Hunan Yi, Alan D. F. Dunbar, Andrew J. Pearson, Darren C. Watters, Tom S. Glen, Andrew C. Brook, James Kingsley, Alastair R. Buckley, Maximilian W. A. Skoda, Athene M. Donald, Richard A. L. Jones, Ahmed Iraqi, and David G. Lidzey**

We report the fabrication of high performance organic solar cells by spray-coating the photoactive layer in air. The photovoltaic blends consist of a blend of carbazole and benzothiadiazole based donor–acceptor copolymers and the fullerene derivative $PC_{70}BM$. Here, we formulate a number of photovoltaic inks using a range of solvent systems that we show can all be deposited by spray casting. We use a range of techniques to characterize the structure of such films, and show that spray-cast films have comparable surface roughness to spin-cast films and that vertical stratification that occurs during film drying reduces the concentration of PCBM towards the underlying PEDOT:PSS interface. We also show that the active layer thickness and the drying kinetics can be tuned through control of the substrate temperature. High power conversion efficiencies of 4.3%, 4.5% and 4.6% were obtained for solar cells made from a blend of $PC_{70}BM$ with the carbazole-based co-polymers PCDTBT, P2 and P1. By applying a low temperature anneal after the deposition of the cathode, the efficiency of spray-cast solar-cells based on a P2:$PC_{70}BM$ blend is increased to 5.0%. Spray coating holds significant promise as a technique capable of fabricating large-area, high performance organic solar cells in air.

Introduction

The finite supply of fossil fuels and escalating energy demands have driven the development of energy from renewable sources such as sun, wind, tide, water and biomass. Organic photovoltaic (OPV) devices convert the energy of sunlight directly into electricity, and have attracted significant attention due to their potential of solution-processability over large-area, mechanically-flexible substrates using low cost manufacturing techniques. Polymer-fullerene bulk heterojunction (BHJ) OPVs now demonstrate power conversion efficiencies (PCE) above 9% in single junction cells.[1]

Under most laboratory conditions, the polymer:fullerene active layer in an OPV is fabricated by spin-casting. However, spin-casting limits the maximum area of the films that can be practically prepared to a few 10's of cm^2 and is also a wasteful technique, as a large amount of material is lost during the process. More importantly, the film nano and meso-structure is highly dependent on film drying kinetics which can significantly affect the ultimate power conversion efficiency of the OPV device. Therefore, any optimization protocol used to create high efficiency devices based on spin-casting cannot be simply translated to a different film deposition process such as inkjet printing, spray-coating or roll-to-roll coating, as the nanostructure developed during the film formation process may be different. It is thus necessary to explore the fabrication of solar cell devices prepared by methods that can be scaled to large-areas, permitting key parameters needed

Dr. T. Wang, N. W. Scarratt, Dr. A. J. Pearson, D. C. Watters, A. C. Brook, Dr. J. Kingsley, Dr. A. R. Buckley, Prof. R. A. L. Jones, Prof. D. G. Lidzey
Department of Physics and Astronomy
University of Sheffield
Sheffield, S3 7RH, UK
E-mail: t.wang@hotmail.com; d.g.lidzey@sheffield.ac.uk

Dr. H. Yi, Dr. A. Iraqi
Department of Chemistry
University of Sheffield
Sheffield, S3 7HF, UK

Dr. A. D. F. Dunbar
Department of Chemical and Biological Engineering
University of Sheffield
Sheffield S1 3JD, UK

T. S. Glen, Prof. A. M. Donald
Cavendish Laboratory
Department of Physics
University of Cambridge
Cambridge CB3 0HE, UK

Dr. J. Kingsley
Ossila Ltd, Kroto Innovation Centre
Broad Lane, Sheffield, S3 7HQ, UK

Dr. M. W. A. Skoda
ISIS Pulsed Neutron and Muon Source
Science and Technology Facilities Council
Rutherford Appleton Laboratory
Harwell Science and Innovation Campus
Didcot OX11 0QX, UK

DOI: 10.1002/aenm.201200713

to optimize device efficiency to be identified; a necessary first step in the design of a practical manufacture strategy.

Previous work on the development of organic solar cells using spray-coating as the active layer deposition method have mainly explored P3HT:PCBM photovoltaic blends.[2–7] A device efficiency of ≤3.0% was reported for P3HT:PCBM solar cells when the active layer was spray cast from a solution of chlorobenzene (CB). A PCE of 3.75% has been reported for spray-cast devices based on P3HT:PCBM,[7] with the film cast from a two-solvent system of orthodichlorobenzene (oDCB) as the primary solvent and mesitylene as the secondary solvent. The use of a secondary solvent having a lower boiling point and lower surface tension has been shown to promote the wettability and uniformity of the P3HT:PCBM film.[4,7] Using a solvent mixture of DCB and CB, a PCE of 4.1% was achieved in P3HT:PCBM solar cells by airbrush spray coating.[8] Other work[9] on spray-coating OPVs using a polymer:fullerene blend composed of the low energy-gap polymer poly[4,8-bis (1-pentylhexyloxy) benzo[1,2-b:4,5-b′]dithiophene-2,6-diylalt-2,1,3-benzoxadiazole -4,7-diyl has reported device with an average PCE of 5.2% (max. 5.8%), indicating that spray-coating is a promising technique to produce high-efficiency devices at low manufacture cost.

In this work, we have studied bulk heterojunction solar cells utilizing three different carbazole and benzothiadiazole based donor–acceptor copolymers, namely PCDTBT, P1 and P2, together with the fullerene derivative $PC_{70}BM$, with the active layer spray-coated in air. We optimize device efficiency by altering the casting solvent, the substrate temperature and the thickness of the active layer. Recent work has also described the fabrication by spray coating of solar cell devices based on the low band gap polymer PCDTBT.[10] However, the PCE achieved was limited to 1.08%; an efficiency that is substantially lower than that obtained when the active layer is instead deposited by spin casting. Here, we report a high power conversion efficiency of 5.0% in P2:$PC_{70}BM$ devices. Optical interferometry and AFM surface analysis show that the spray-coated active layer has comparable surface roughness to films deposited by spin-casting. Neutron scattering measurements indicate a relative depletion of $PC_{70}BM$ near the PEDOT:PSS layer interface in the PCDTBT:$PC_{70}BM$, P1:$PC_{70}BM$ and P2:$PC_{70}BM$ blends. Controlling the vertical distribution of such components appears a promising strategy for further improvement in device efficiency.

Results and Discussion

Figure 1(a) shows the molecular structure of the donor–acceptor copolymers used in this work. These materials were synthesized according to previously reported methods.[11] The HOMO and LUMO levels of P1 are –5.40 eV and –3.27 eV respectively, with values for P2 and PCDTBT being (–5.20 eV and –3.29 eV) and (–5.35 eV and –3.42 eV) respectively. The optical energy-gap of PCDTBT, P1 and P2 are 1.88, 1.98 and 1.93 eV, respectively. The differing electronic properties of these molecules derive from the different repeat units along their molecular backbones.[11]

The spray coater employed in this work is a Prism 300 supplied by Ultrasonic Systems, Inc. Previous work has mainly used spray coaters that have a nozzle, inside which micron scale droplets are generated using an ultrasonic transducer.[2,5,7]

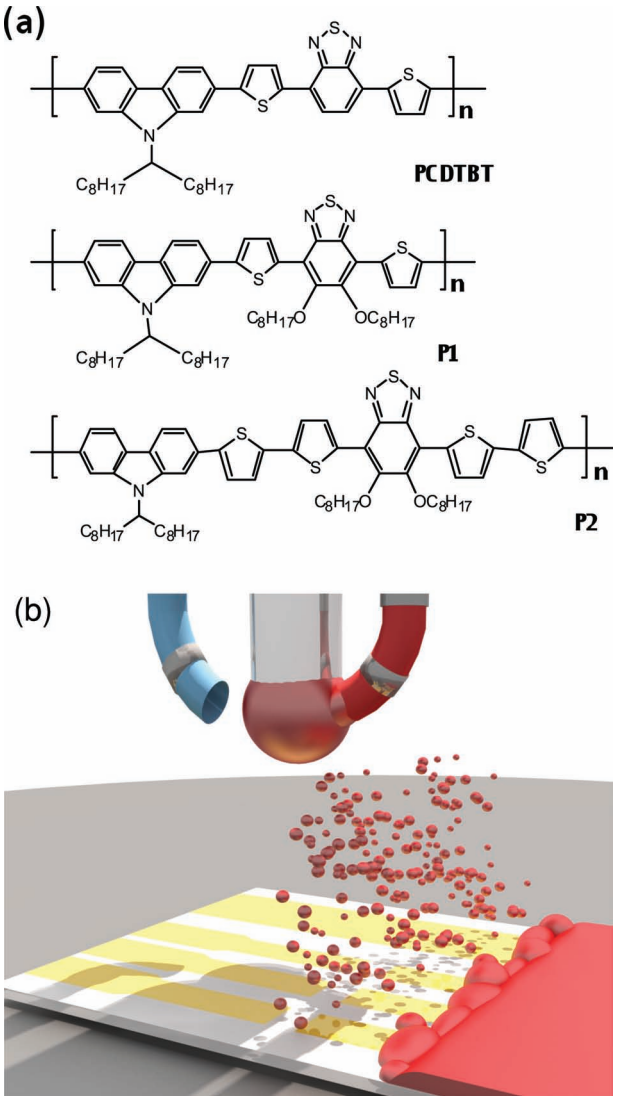

Figure 1. (a) Molecular structures of carbazole and benzothiadiazole based donor–acceptor copolymers, PCDTBT, P1 and P2. (b) A diagram of spray casting using a nozzle-less ultrasonic spray coater.

The spray coater employed in this work is, however, nozzle-less. Figure 1(b) shows a schematic of the spray coating process. Here, the photovoltaic blend solution is delivered to a tip that is vibrated using a piezoelectric crystal at 35 kHz. The ultrasonic vibration breaks the solution into micron-sized droplets, with a low-pressure gas stream being used to shape and focus the droplets into a spray that is directed towards the substrate. This technique is different from the nozzle-based spray-coating systems previously explored in which the primary droplets that are generated in the nozzle can coalesce to form larger secondary droplets before being deposited on the target surface. The nozzle-less spray coating method employed here can substantially reduce the process of droplet coalescence, and is therefore better suited to the generation of a very fine aerosol, which–as we show–permits nanoscale films to be deposited with high precision. We have formulated a range of polymer-fullerene ink solutions that are based on a single solvent or a

Table 1. Surface tension (γ) of PCDTBT:$PC_{70}BM$ (1:4) solutions(4 mg/ml) and the contact angles (θ) on PEDOT:PSS film at room temperature.

	CB	DCB	DCB:CB (1:1)	DCB:CF (7:3)	DCB:CF (6:4)	DCB:CF (5:5)	DCB:CF (4:6)	DCB:CF (3:7)
γ (mN m^{-1})	29	31.3	30.8	31.5	29.8	31.0	29.8	31.5
θ (°)	3.5	1.2	1.8	1.8	1.8	1.2	2.6	2.9

mixture of solvents to deposit thin films by spray coating. The polymer:fullerene blends are fixed at 1:4 (w/w) which is the optimum blending ratio identified from our previous study.[11] In all cases, a solid content of 4 mg/ml was found to be sufficient to create films having a thickness between 50 and 100 nm created using a single spray-coat pass in air. Control devices fabricated by spin-casting the active layer in air were also explored. We find that processing devices in air does not have a negative impact on the efficiency of PCDTBT:$PC_{70}BM$ photovoltaic devices. Device optimization was performed on the various photovoltaic blends through the choice of solvent, the device substrate temperature during the spray-coating process and the final thickness of the active layer. We avoid the use of a single solvent with a low boiling point such as chloroform (CF) as our experiments demonstrated that the rapid evaporation of CF causes spray droplets to partially dry before they reach the substrate. Such droplets do not coalesce to form a uniform thin film, but form a film characterized by pin-holes and the presence of micron and nanometer-sized particles separated by many sub-micron scale interfaces. We find such films perform very poorly in OPV applications. The various PCDTBT:$PC_{70}BM$ solutions explored are outlined in **Table 1**, together with their surface tension and contact angle on a PEDOT:PSS substrate. The surface tension of solutions were measured using the pendant drop method and were found to be ~ (30 ± 2) mN m^{-1} at room temperature. Contact angles were recorded dynamically as a solution drop expanded and then stabilized upon wetting the PEDOT:PSS surface. In general, a large surface tension and contact angle usually leads to a poor wettability of the solution on the substrate, causing the film to undergo dewetting as it dries. The data shown in Table 1 indicates that the stabilized contact angle of the ink drops explored are between 1 and 4°, indicating excellent wettability on PEDOT:PSS. This is confirmed experimentally as we find that spray-coated droplets rapidly coalesce to form a uniform wet film. However, we find that at room temperature, such films shrink progressively towards the center of the substrate. To reduce such shrinkage, we have explored spray-casting onto a heated substrate. This procedure shortens the drying time of the spray coated active layer to between 30 seconds and 1 minute, and thus minimizes film shrinkage. We discuss the role of such a process on determining film efficiency in a later section.

We have explored the morphology of spray-cast photovoltaic blends over length-scales ranging from 10s of nm to 100s of µm using scanning force microscopy and optical interferometry. **Figures 2**(a) and (c) show the surface topography of a PCDTBT:$PC_{70}BM$ film fabricated by spray-casting from CB onto a substrate held at 40 °C. Here, parts (a) and (c) were recorded

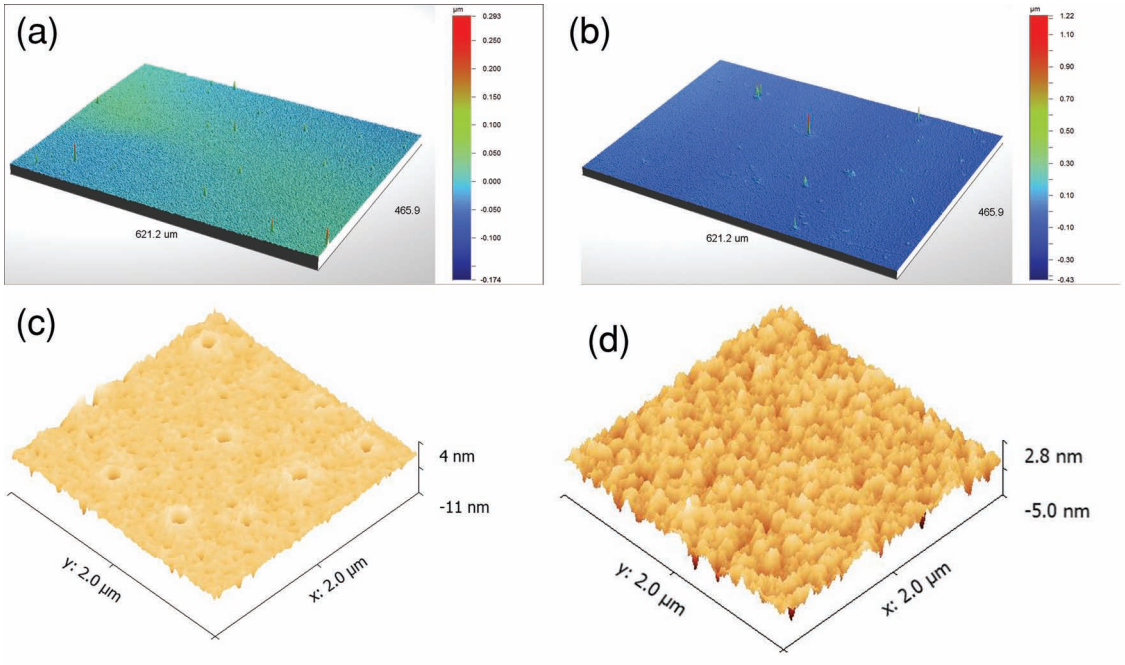

Figure 2. (a) 3D optical interferometry and (c) AFM images of a PCDTBT:$PC_{70}BM$ (1:4) films spray cast from CB onto a substrate held at a temperature of 40 °C. (b) 3D optical interferometry and (d) AFM images of PCDTBT:$PC_{70}BM$ (1:4) films spin-cast from CB at room temperature. The size of the optical interferometry images is approximately 620 µm × 470 µm.

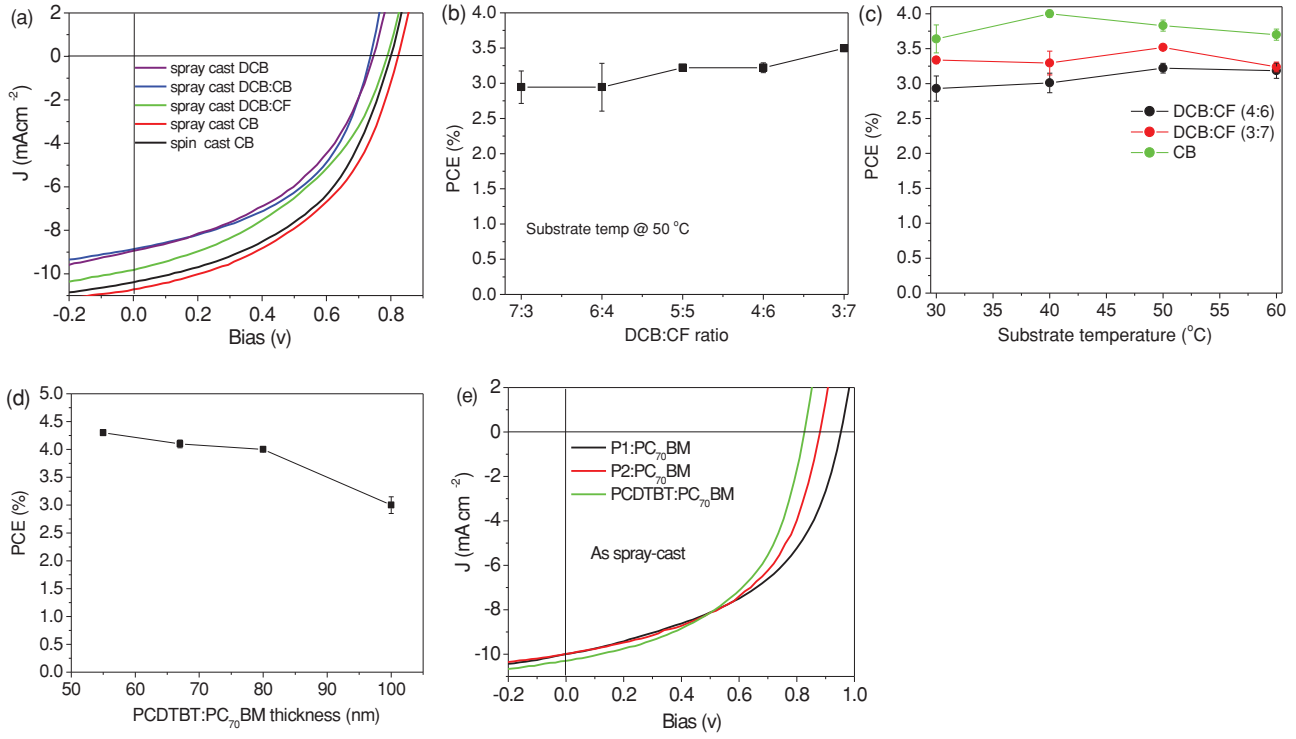

Figure 3. (a) J–V curves of PCDTBT:PC_{70}BM devices fabricated by spray-coating from different solvents. The J-V curve of a control device formed from spin-casting is also shown. (b)The effect of the DCB:CF blend ratio on device efficiency. (c) The effect of substrate temperature on device efficiency for a PCDTBT:PC_{70}BM OPV spray-coated from a CB solution. (d) The recorded PCE as a function of active layer thickness for PCDTBT:PC_{70}BM devices spray-coated from CB solution. (e) J-V curves of P1:PC_{70}BM, P2:PC_{70}BM, and PCDTBT:PC_{70}BM devices spray-coated from CB solutions at an optimum substrate temperature of 40 °C.

using optical interferometry and AFM respectively. Parts 2(b) and (d) show surface topography of a film spin-cast from CB recorded using optical interferometry and AFM. It can be seen that the spray cast film is highly uniform over a length-scale of 100s of μm and does not contain obvious grain boundaries, or the remnants of individual spray droplets. The RMS (root-mean-square) roughness of the spray-cast film evaluated over an area of 620 μm × 470 μm is 15 nm. The surface RMS roughness of the spin-cast film determined over a similar area is 13 nm. We believe that this is because during a single-pass spray deposition process, the individual droplets that reach the substrate coalesce into a continuous wet layer before drying into a homogeneous thin film. This process leads to the formation of films having a relatively low surface roughness, characterized by RMS values that are not much greater than those of spin cast films. The similarity in film structure at smaller length-scales (2 μm × 2 μm) is again confirmed using AFM; here we record a peak-to-valley roughness of around 14 nm for the spray-cast film and 8 nm for the spin-cast film.

Figure 3(a) shows typical *J–V* curves of PCDTBT:PC_{70}BM devices having an active layer thickness of around 80 nm deposited by spray-coating from different solutions. In this experiment, films are coated at different (optimized) temperatures. We summarize such temperatures together with representative device metrics in **Table 2**. For comparison, Figure 3(a) also plots data recorded from a control device having a 75 nm thick active layer that was spin-cast from CB. We find that the PCEs of devices spray-cast from DCB, DCB:CB and DCB:CF solutions are between 3.0 and 3.2%, having a V_{oc} above 0.75 V and a *FF* below 50%. A much higher device PCE of 4.0% is achieved when the active layer is spray-coated from CB, with a J_{sc} of 10.7 mA/cm^2, a V_{oc} of 0.82 V and a *FF* of 46%. It is clear that the casting solvent affects the device V_{oc} when other film preparation parameters are kept the same. This effect has also been observed in PCBTDPP:PCBM[12]

Table 2. Device metrics of PCDTBT:PC_{70}BM OPVs fabricated by spray and spin casting from different solvents.

Method	Solvent	Optimum Substrate temp (°C)	Thickness (nm)	J_{sc} (mA/cm^2)	V_{OC} (V)	*FF* (%)	*PCE* (%)
Spray-cast	DCB	80	~80	8.95	0.75	45	3.0
Spray-cast	DCB:CB (1:1)	80	~80	8.86	0.75	48	3.1
Spray-cast	DCB:CF (1:1)	50	~80	9.73	0.79	42	3.2
Spray-cast	CB	40	~80	10.70	0.82	46	4.0
Spin-cast	CB	RT	~75	10.50	0.80	47	3.9

and pBBTDPP2:PCBM[13] blends based solar-cells. Here, the casting solvent plays a significant role in determining the eventual nanostructure of the photovoltaic blends and can affect the effective HOMO level of the polymer and the LUMO level of the PCBM and thereby, modify the V_{oc} of a device.[14,15] From the results presented in Figure 3(a) and Table 2 it can be seen that the control device having an active layer prepared by spin casting from CB has a PCE (3.9%) that is very similar to its spray-cast analogue. This demonstrates that devices incorporating a spray-cast active layer can operate with similar efficiency compared with devices in which the active layer is spin-cast.

Previous work on P3HT:PCBM solar cells fabricated using spray-coating from a solvent mixture resulted in devices having higher efficiency than those cast from a single solvent system.[4] Our results suggest however that PCDTBT:PC_{70}BM solar cells spray-cast from a mixture of solvents are characterized by a lower PCE. We note that the drying time of a PCDTBT:PC_{70}BM film spray cast from the different solvents at their optimum substrate temperature are all around 1 minute. This drying time is substantially faster than those used to spray coat P3HT:PCBM solar cells,[7] which is often more than 5 minutes. As P3HT is a semi-crystalline polymer, it has been demonstrated that enhanced crystallinity contributes to increased optical light absorption,[16] enhanced charge separation,[17,18] improved charge transport[19] and consequently improved device efficiency. The extended drying times using a high boiling point solvent in the solvent mixture clearly allows P3HT to undergo a greater degree of crystallization during the film formation process and thereby results in improved device performance. PCDTBT is however largely amorphous in an as-cast solid state,[20,21] and thus a PCDTBT:PC_{70}BM blend does not need an extended drying time in order to drive self-organization.

In Figure 3(b), we summarize the effect of the DCB:CF solvent blend ratio on device efficiency for PCDTBT:PC_{70}BM devices spray-cast on a substrate held at 50 °C. Here, relevant device metrics are summarized in Supporting Information in Table S1. It can be seen that the solvent blend ratio affects both device performance and pixel-to-pixel repeatability. Indeed, the standard deviation of device efficiency is reduced from around 0.3% for devices cast from a solvent blend in which DCB is in excess, to less than 0.1% once the DCB:CF ratio is equal to or less than 1:1; an effect that we believe reflects improved film uniformity. We find that device PCE increases slightly as more CF solvent is incorporated into the ink, with device efficiency reaching 3.5% when the blend solution consists of a DCB:CF ratio of 3:7 (volume ratio). This increase in efficiency results from an increase in the V_{oc} to 0.82 V and a slightly higher *FF* of 45% compared with devices cast at other DCB:CF blend ratios. However when the CF concentration is in large excess, spray-cast films undergo a phenomenon similar to that of dewetting. As the boiling points of CF and DCB are 62 and 180 °C respectively, we suspect that the large difference in the evaporation rates of CF and DCB leads to non-uniform lateral drying in films. This process leads to fast evaporation of CF generating regions that are almost "dry" and encourages a local flow of DCB from surrounding regions toward such "dried" regions. This process is however not fast enough to maintain a uniform solvent distribution during drying and results in highly non-uniform films.

We have explored the effect of the temperature of the substrate on which the film is spray-cast and summarize the optimum substrate temperatures for PCDTBT:PC_{70}BM films spray-cast using different solvents in Table 2. In general, we find that a higher substrate temperature reduces the film drying time and minimizes the shrinkage of the wet film (thereby improving its uniformity), however the film drying kinetics will influence the nanoscale morphology and therefore impact on device efficiency. Indeed, previous work has demonstrated that a substrate temperature of 55 °C was effective in improving the device efficiency of P3HT:PCBM based solar cells.[4,7] Here, we found that substrate temperature has some effect on device efficiency, as summarized in Figure 3(c). Here the active layer was cast from either CB or DCB:CF blend at the volume ratios of 4:6 and 3:7. We find that optimum device efficiency is achieved when the substrate is held at a temperature of 40 and 50 °C for PCDTBT:PC_{70}BM films spray-cast from CB and DCB:CF solutions respectively. However, a higher temperature of 80 °C is necessary to obtain optimal efficiency for devices cast from DCB and DCB:CB.

The results presented in Figure 3(a) and summarized in Tables 2 and S1 suggest that devices spray cast from a pure CB solution are in fact more efficient compared with those spray-cast from the other solution blends that have been explored. We have therefore concentrated on optimizing devices spray-cast from CB alone by adjusting the thickness of the active layer, achieved by varying the tip-to-substrate distance during spray-casting. Figure 3(d) summarizes the effect of PCDTBT:PC_{70}BM active layer thickness over the range of 55 to 100 nm on device efficiency with device metrics summarized in Table S2. We find that the device efficiency increases as the active layer becomes thinner, with the highest PCE of 4.3% for an active layer thickness of 55 nm; a value that reduces to 3.0% as the thickness of the active layer is increased to 100 nm. It is known that PCDTBT is a largely amorphous polymer, characterized by some π–π stacking in an as-cast state.[20,21] This amorphous nature results in relatively poor charge mobility necessitating the use of thin films for efficient charge extraction,[22] with charge carrier trapping and fast bimolecular recombination limiting photovoltaic efficiency in devices based on 'thick' (>100 nm) PCDTBT:PCBM films.[23–25] Our results (see Table S2) also suggest that the *FF* reduces linearly as the active layer thickness increases, going from 51% in the devices based on a 55 nm thick active layer, to 40% in devices with a 100 nm active layer, a result qualitatively consistent with studies on PCDTBT:PCBM[26,27] and MDMO-PPV:PCBM[28] OPV devices.

In order to understand the generality of the processing methodologies investigated in this work, we have explored the use of spray-coating to deposit thin films of P1:PC_{70}BM and P2:PC_{70}BM. Here, films were spray cast from CB at a solid content of 4 mg/ml, onto a device substrate held at a range of temperatures. We again find an optimum substrate temperature of around 40 °C for both blends; a value similar to that used to create optimized PCDTBT based OPVs when spray-coated from CB. We find that the surface roughness of such films is very similar to that of a PCDTBT:PC_{70}BM film prepared from spray coating. This is confirmed by AFM images of P1:PC_{70}BM and P2:PC_{70}BM blends that we presented in the supporting information Figure S1.

Table 3. Devices metrics for films prepared by spray-casting from a CB solvent onto a substrate held at a temperature of 40 °C. TA indicates that films have been thermally annealed at 80 °C.

Method	Materials	Thickness (nm)	J_{sc} (mA/cm^2)	V_{oc} (V)	*FF* (%)	*PCE* (%)
Spray-cast	PCDTBT:$PC_{70}BM$	~55	10.08	0.84	51	4.3
Spray-cast + TA	PCDTBT:$PC_{70}BM$	~55	10.33	0.86	51	4.5
Spray-cast	P1:$PC_{70}BM$	~78	10.00	0.95	49	4.6
Spray-cast+ TA	P1:$PC_{70}BM$	~78	10.04	0.94	48	4.5
Spray-cast	P2:$PC_{70}BM$	~76	10.00	0.88	51	4.5
Spray-cast+ TA	P2:$PC_{70}BM$	~76	10.23	0.90	54	5.0

In Figure 3(e) we plot J-V curves of P1:$PC_{70}BM$ and P2:$PC_{70}BM$ devices, together with that of a PCDTBT:$PC_{70}BM$ device with device metrics summarized in **Table 3**. In all cases, data is presented from devices having an optimum active-layer thickness. It can be seen that P1:$PC_{70}BM$ and P2:$PC_{70}BM$ devices have a higher PCE compared to those of PCDTBT:$PC_{70}BM$ devices, being 4.6% and 4.5%, respectively. This improvement in PCE is mainly due to increased V_{oc}, with the maximum V_{oc} in devices made from PCDTBT, P2 and P1 being 0.84, 0.88 and 0.95V, respectively. This trend of increased V_{oc} is qualitatively similar to our previous study on these materials when fabricated into OPV devices by spin-casting.[11]

We can promote further improvement in device PCE by thermal annealing spray-coated devices at 80 °C for 10 minutes after the cathode layer has been deposited. This process (summarized in Table 3) appears relatively effective in PCDTBT:$PC_{70}BM$ and P2:$PC_{70}BM$ devices, however is of negligible benefit in P1:$PC_{70}BM$ devices. We find the PCE of P2:$PC_{70}BM$ OPV is improved to 5.0% after a post deposition "low temperature" thermal anneal. This observation is consistent with previous work on PCDTBT solar cells in which a low temperature thermal treatment was shown to increase relative device performance by around 5 to 10%.[29–31] We note that thermal annealing of PCDTBT at a temperature above its glass transition (around 130 °C) will reduce π–π stacking,[20,21] however annealing at a temperature around 70 °C can in fact promote π–π stacking.[20] We believe that the slightly increased structural order that results from this "low temperature" anneal may explain the improved device performance observed here.

Finally, we have used neutron scattering to characterize the vertical distribution of $PC_{70}BM$ in the different blends fabricated by spray-coating. We have previously used this technique to characterize spin-cast films of PCDTBT:$PC_{70}BM$, and have evidenced an enrichment of $PC_{70}BM$ at the film surface.[32] **Figure 4**(a) shows the neutron reflectivity of PCDTBT:$PC_{70}BM$ blend films spray cast from a CB solution onto a substrate held at a temperature of 40, 60 and 80 °C. The reflectivity data is fitted using a slab model consists of multiple thin recursive layers. In the model, the layer representing the photovoltaic blend was described by either one or two slabs to account for enrichment/depletion at the air-blend and blend-PEDOT:PSS interfaces. The quality of the model was then verified using an N-sigma analysis (based on the Hamilton test),[33,34] which weights the obtained goodness-of-fit by the number of data points and free parameters. In all case a two-slab model for the photovoltaic blend was necessary for the description of the stack.

Figure 4(b) plots the corresponding scattering length density (SLD) profiles. In the figure, we identify the location of the Si/SiOx, PEDOT:PSS and PCDTBT:$PC_{70}BM$ interfaces. The SLDs of PCDTBT, $PC_{70}BM$ and PEDOT:PSS used in our calculations are 1.19×10^{-6}, 4.42×10^{-6} and 1.80×10^{-6} Å^{-1} respectively as calculated using the NIST online database.[35] Note, the high SLD of SiOx is evidenced by a distinct peak located between the PEDOT:PSS and Si layers. It can be seen that the films studied have a similar (but not identical) thickness. The profiles shown in Figure 4(b) indicate that the modeled film roughness at the air interface is around 10 nm; a result quantitatively similar with the values obtained using optical interferometry and AFM. It can be seen that the surface of the films (the air-interface) are significantly enriched in $PC_{70}BM$. For example, for PCDTBT:$PC_{70}BM$ films cast at a substrate temperature of 40 °C, we find that the first 80 nm of film is characterized by an average SLD of 4.1×10^{-6} Å^{-1}, indicating that at this point, the blend is composed of approximately 90% $PC_{70}BM$ by mass. This is consistent with strong surface segregation of $PC_{70}BM$ as reported previously.[32] It can be seen however that the $PC_{70}BM$ concentration becomes relatively depleted towards the PEDOT:PSS interface. Our fitting indicates that the width of this depleted region is around 17 nm and has a roughness around 6 nm. The SLD of this depleted region close to the PEDOT:PSS interface is *ca.* 3.3×10^{-6} Å^{-1}, indicating a local $PC_{70}BM$ concentration of 65% by mass. As the substrate temperature during film casting is increased from 40 to 60 °C, the width of the depleted region is reduced to around 13 nm and has an associated roughness of around 7nm. The SLD of the depleted region is concomitantly increased to 3.7×10^{-6} Å^{-1}, indicating a $PC_{70}BM$ mass concentration of 78%. For blend films spray-cast onto a substrate held at 80 °C, the depletion of $PC_{70}BM$ at the PEDOT:PSS is practically suppressed, with the $PC_{70}BM$ concentration at this point approaching that of the bulk. Our neutron reflectivity results suggest therefore that the volume of the $PC_{70}BM$ depleted region reduces as the substrate temperature is increased; a phenomenon that most likely results from the faster drying dynamics that occurs at elevated temperatures, suppressing vertical stratification in the drying film. Such a relative depletion of $PC_{70}BM$ near the PEDOT:PSS is clearly beneficial for efficient hole extraction into the PEDOT:PSS layer. We speculate that the reduced volume of the $PC_{70}BM$ depleted region in films deposited at higher temperature partially explains the slightly reduced performance of devices spray-coated at elevated temperatures (see Figure 3c). It is also important to recognize however that a rapid film drying rate may also result in the existence of a series of loosely-connected nanoparticles within the film, as the spray droplets have not had sufficient time to coalesce. This effect is likely to decrease charge carrier mobility and thereby reduce device efficiency.

In Figures 4(c) and 4(d), we present neutron reflectivity measurements recorded from P1:$PC_{70}BM$ and P2:$PC_{70}BM$ films spray-coated from CB onto a substrate held at 40 °C. It is clear that the film is also characterized by a $PC_{70}BM$ depleted region close to the PEDOT:PSS interface. Interestingly, it appears that the reduction of the $PC_{70}BM$ concentration towards the PEDOT:PSS interface is relatively larger in blends

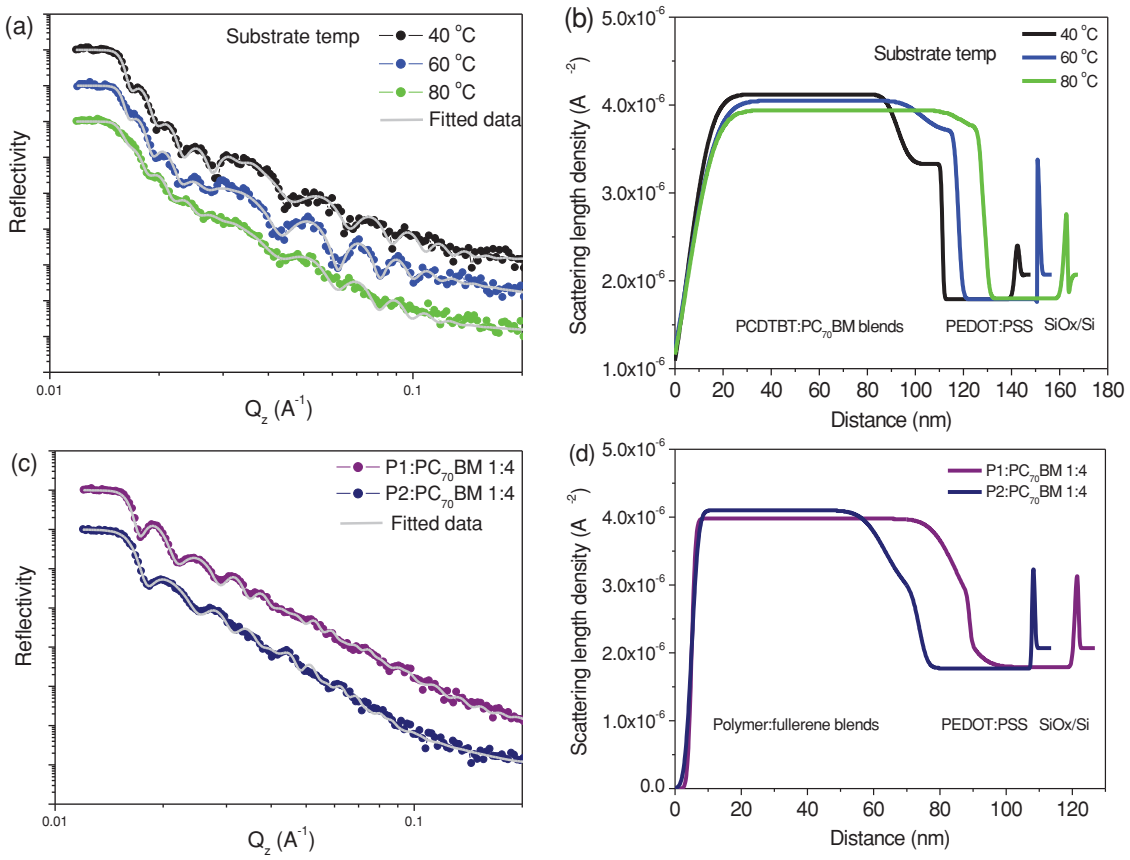

Figure 4. (a) Neutron scattering reflectivity and (b) scattering length density profiles of PCDTBT:$PC_{70}BM$ (1:4) blends deposited by spray-coating at three different substrate temperatures from a CB solution. (c) Neutron scattering reflectivity and (d) scattering length density profiles of P1:$PC_{70}BM$ and P2:$PC_{70}BM$ blends deposited by spray-coating at a substrate temperature of 40 °C from a CB solution. The thicknesses of the blend films are slightly different for the samples.

based on P1 and P2 compared to blends based on PCDTBT. The reason for such difference in interface structure is not yet understood, however it appears a depletion of $PC_{70}BM$ towards the underlying PEDOT:PSS interface appears a general feature of blends of a fullerene with carbazole and benzothiadiazole based donor–acceptor copolymers. The exact width and extent of the depleted region is apparently sensitive to the deposition conditions, presenting an opportunity to tailor the vertical distribution and thereby enhance the hole and electron extraction properties of such photovoltaic systems.

Conclusions

We have formulated various organic inks containing photovoltaic blends of three different carbazole-based donor–acceptor conjugated copolymers that can be deposited by spray-coating in air. We find that spray-coated films have comparable surface roughness compared to those deposited by spin-casting. We optimize device efficiency through varying the casting solvent, the substrate temperature and the thickness of the active layer. A PCE of 4.6% is achieved from devices spray-coated from a blend of P1 and $PC_{70}BM$, with a maximum device efficiency of 5.0% recorded following a subsequent post-cathode thermal anneal for a P2:$PC_{70}BM$ based device. Neutron reflectivity measurements indicate that a depletion of the $PC_{70}BM$ towards the underlying anode appears a general feature of blends based on polycarbazole co-polymers blended with functionalized fullerenes. Such vertical stratification is anticipated to be beneficial for applications in OPV devices. Our results indicate that spray-coating is a technique capable of producing high efficiency organic photovoltaic devices and combines the advantages of low-cost deposition over large areas under ambient conditions.

Experimental Section

PCDTBT, P1 and P2 had an M_w and PDI of 26.5 kDa and 2.18, 54.1 kDa and 2.16, 57.2 kDa and 1.84 respectively. Blend films were coated using a Prism ultrasonic spray-coating system supplied by Ultrasonic Systems, Inc. (USI). This system uses a fixed ultrasonic frequency of 35 kHz and a nitrogen-gas carrier pressure of 10 psi. To characterize wetting and dewetting of the various solutions, the surface tension of the solutions were measured via the pendant drop method using a Theta Optical Tensiometer. Dynamic contact angles of the solution drops on a PEDOT:PSS surface at room temperature were also measured using the same system with the average value for the stabilized contact angle reported in this work. Spectroscopic ellipsometry using a M2000v system supplied by J. A. Woollam Co. was used to determine the thickness of the PCDTBT:$PC_{70}BM$ layer on a silicon/PEDOT:PSS substrate. Optical

interferometry measurements were performed using a Veeco optical interferometer. Neutron reflectivity measurements were performed on the INTER reflectometer at the ISIS pulsed neutron source at the Rutherford Appleton Laboratory, UK.[36] The available wavelength range was 1.5 to 15 Å and the reflectivity was measured at two different angles (0.5 and 2.3°) and the data combined to give a q range of 0.012 $Å^{-1}$ to 0.2 $Å^{-1}$. Beyond this range the reflectivity was dominated by the background. The experimental resolution was constant at $\Delta q/q = 0.03$. The NR data were analyzed using a slab model stacked with multiple thin layers, with each layer assigned a thickness, roughness and a scattering length density (SLD). The data were fitted using a least-squares fit.

OPV devices were defined on pre-patterned ITO substrates provided by Ossila Ltd. The ITO/glass substrates were first cleaned by sonication in dilute NaOH followed by IPA. The size of the ITO/glass substrate used in this work was 20 × 15 mm^2, on to which six pixels are defined, each having an area of 4.5 mm^2. A 30 nm PEDOT:PSS (HC Starck Clevios P AI4083) anode layer was spin cast in air on the ITO/glass substrate. The PEDOT:PSS films were annealed for one minute at 110 °C to evaporate any absorbed moisture. The PCDTBT:PC_{70}BM, P1:PC_{70}BM, P2:PC_{70}BM active layers were spray-coated in air onto the glass/ITO/PEDOT:PSS substrate that was held on a hot plate. The substrate temperature, tip-to-substrate distance, and the casting solvent were varied in order to change the morphology and thickness of the active layer. Control spin-cast films were also coated in air. All films were then transferred to an over pressure nitrogen glovebox connected to a thermal evaporator system for deposition of the OPV cathode (5 nm of calcium capped by a 100 nm of aluminum evaporated at a base pressure of ~10^{-7} mbar). The cathode deposition was made through a shadow-mask, producing a series of independent devices. The active area of each device is defined by the overlap between the anode and the cathode, which we estimate to be 4.8 mm^2. Devices were finally encapsulated using a glass slide and epoxy glue before testing. PCEs were determined using a Newport 92251A-1000 AM1.5 solar simulator. An NREL calibrated silicon cell was used to calibrate the power output to 100mW cm^{-2} at 25 °C.

Supporting Information

Supporting Information is available from the Wiley Online Library or from the author.

Acknowledgements

We thank financial support from EPSRC via grant EP/I028641/1 "Polymer/fullerene photovoltaic devices: new materials and innovative processes for high-volume manufacture". AJP thanks King Abdulaziz University under grant no. D-004/431 for financial support. We thank Dr. David Coles (University of Sheffield) for preparing Figure 1b. We thank Dr. Tim Richardson and Dr. Stuart Brittle for assistance with the surface tension and contact angle measurements. We also thank Amit Rana (University of Sheffield), Chris Saywell and Michelle Morgan (FaraPack Polymers Ltd) for assistance with the optical interferometry measurements.

Received: September 10, 2012
Revised: November 15, 2012
Published online: February 5, 2013

[1] Z. He, C. Zhong, S. Su, M. Xu, H. Wu, Y. Cao, *Nature Photonics* **2012**, *6*, 593.
[2] D. Vak, S.-S. Kim, J. Jo, S.-H. Oh, S.-I. Na, J. Kim, D.-Y. Kim, *Appl. Phys. Lett.* **2007**, *91*, 081102.
[3] C. Girotto, B. P. Rand, J. Genoe, P. Heremans, *Sol. Energy Mater. Sol. cells* **2009**, *93*, 454.
[4] C. N. Hoth, R. Steim, P. Schilinsky, S. A. Choulis, S. F. Tedde, O. Hayden, C. J. Brabec, *Org. Electron.* **2009**, *10*, 587.
[5] K. X. Steirer, M. O. Reese, B. L. Rupert, N. Kopidakis, D. C. Olson, R. T. Collins, D. S. Ginley, *Sol. Energy Mater. Sol. cells* **2009**, *93*, 447.
[6] L.-M. Chen, Z. Hong, W. L. Kwan, C.-H. Lu, Y.-F. Lai, B. Lei, C.-P. Liu, Y. Yang, *ACS Nano* **2010**, *4*, 4744.
[7] C. Girotto, D. Moia, B. P. Rand, P. Heremans, *Adv. Funct. Mater.* **2011**, *21*, 64.
[8] G. Susanna, L. Salamandra, T. M. Brown, A. D. Carlo, F. Brunetti, A. Reale, *Sol. Energy Mater. Sol. cells* **2011**, *95*, 1775.
[9] W. Nie, R. C. Coffin, J. Liu, Y. Li, E. D. Peterson, C. M. MacNeill, R. E. Noftle, D. L. Carroll, *Appl. Phys. Lett.* **2012**, *100*, 083301.
[10] L. Saitoh, R. R. Babu, S. Kannappan, K. Kojima, T. Mizutani, S. Ochiai, *Thin Solid Films* **2012**, *520*, 3111.
[11] H. Yi, S. Al-Faifi, A. Iraqi, D. C. Watters, J. Kingsley, D. G. Lidzey, *J. Mater. Chem.* **2011**, *21*, 13649.
[12] R. B. Aich, Y. Zou, M. Leclerc, Y. Tao, *Org. Electron.* **2010**, *11*, 1053.
[13] M. M. Wienk, M. Turbiez, J. Gilot, R. A. J. Janssen, *Adv. Mater.* **2008**, *20*, 2556.
[14] P. P. Boix, M. M. Wienk, R. A. J. Janssen, G. Garcia-Belmonte, *J. Phys. Chem. C* **2011**, *115*, 15075.
[15] W. C. Tsoi, S. J. Spencer, L. Yang, A. M. Ballantyne, P. G. Nicholson, A. Turnbull, A. G. Shard, C. E. Murphy, D. D. C. Bradley, J. Nelson, J.-S. Kim, *Macromolecules* **2011**, *44*, 2944.
[16] T. Erb, U. Zhokhavets, G. Gobsch, S. Raleva, B. Stühn, P. Schilinsky, C. Waldauf, C. J. Brabec, *Adv. Funct. Mater.* **2005**, *15*, 1193.
[17] T. M. Clarke, A. M. Ballantyne, J. Nelson, D. D. C. Bradley, J. R. Durrant, *Adv. Funct. Mater.* **2008**, *18*, 4029.
[18] R. A. Marsh, J. M. Hodgkiss, S. Albert-Seifried, R. H. Friend, *Nano Lett.* **2010**, *10*, 923.
[19] V. D. Mihailetchi, H. X. Xie, B. de Boer, L. J. A. Koster, P. W. M. Blom, *Adv. Funct. Mater.* **2006**, *16*, 699.
[20] T. Wang, A. J. Pearson, A. D. F. Dunbar, P. A. Staniec, D. C. Watters, H. Yi, A. J. Ryan, R. A. L. Jones, A. Iraqi, D. G. Lidzey, *Adv. Funct. Mater.* **2012**, *22*, 1399.
[21] Z. M. Beiley, E. T. Hoke, R. Noriega, J. Dacuna, G. F. Burkhard, J. A. Bartelt, A. Salleo, M. F. Toney, M. D. McGehee, *Adv. Energy Mater.* **2011**, *1*, 954.
[22] S. H. Park, A. Roy, S. Beaupre, S. Cho, N. Coates, J. S. Moon, D. Moses, M. Leclerc, K. Lee, A. J. Heeger, *Nat. Photon.* **2009**, *3*, 297.
[23] F. Etzold, I. A. Howard, R. Mauer, M. Meister, T.-D. Kim, K.-S. Lee, N. S. Baek, F. D. R. Laquai, *J. Am. Chem. Soc.* **2011**, *133*, 9469.
[24] T. M. Clarke, J. Peet, A. Nattestad, N. Drolet, G. Dennler, C. Lungenschmied, M. Leclerc, A. J. Mozer, *Org. Electron.* **2012**, *13*, 2639.
[25] Z. Li, C. R. McNeill, *J. Appl. Phys.* **2011**, *109*, 074513.
[26] J. S. Moon, J. Jo, A. J. Heeger, *Adv. Energy Mater.* **2012**, *2*, 304.
[27] D. C. Watters, J. Kingsley, H. Yi, T. Wang, A. Iraqi, D. Lidzey, *Org. Electron.* **2012**, *13*, 1401.
[28] M. Lenes, L. J. A. Koster, V. D. Mihailetchi, P. W. M. Blom, *Appl. Phys. Lett.* **2006**, *88*, 243502.
[29] J. H. Seo, A. Gutacker, Y. Sun, H. Wu, F. Huang, Y. Cao, U. Scherf, A. J. Heeger, G. C Bazan, *J. Am. Chem. Soc.* **2011**, *133*, 8416.
[30] K. X. Steirer, P. F. Ndione, N. E. Widjonarko, M. T. Lloyd, J. Meyer, E. L. Ratcliff, A. Kahn, N. R. Armstrong, C. J. Curtis, D. S. Ginley, J. J. Berry, D. C. Olson, *Adv. Energy Mater.* **2011**, *1*, 813.
[31] D. H. Wang, D. Y. Kim, K. W. Choi, J. H. Seo, S. H. Im, J. H. Park, O. O. Park, A. J. Heeger, *Angew. Chem. Int. Ed.* **2011**, *50*, 5519.
[32] P. A. Staniec, A. J. Parnell, A. D. F. Dunbar, H. Yi, A. J. Pearson, T. Wang, P. E. Hopkinson, C. Kinane, R. M. Dalgliesh, A. M. Donald, A. J. Ryan, A. Iraqi, R. A. L. Jones, D.G. Lidzey, *Adv. Energy Mater.* **2011**, *1*, 499.
[33] J. Ihringer, *J. Appl. Crystallogr.* **1995**, *28*, 618.
[34] W. C. Hamilton, *Acta Cryst.* **1965**, *18*, 502.
[35] http://www.ncnr.nist.gov/resources/sldcalc.html. (Accessed September 2012.)
[36] J. Webster, S. Holt, R. Dalgliesh, *Physica B* **2006**, *1164*, 385–386.